Applied Catalysis B: Environmental 178 (2015) 170–176

Contents lists available at ScienceDirect

Applied Catalysis B: Environmental

journal homepage: www.elsevier.com/locate/apcatb

Zinc sulfide functionalized with ruthenium nanoparticles for photocatalytic reduction of CO_2

Tomasz Baran[a,b], Szymon Wojtyła[a], Angela Dibenedetto[b,c], Michele Aresta[c,d], Wojciech Macyk[a,*]

[a] Faculty of Chemistry, Jagiellonian University in Krakow, ul. Ingardena 3, 30-060 Kraków, Poland
[b] Department of Chemistry, University of Bari, via Orabona 4, 70125 Bari, Italy
[c] CIRCC, via Ulpiani 27, 70126 Bari, Italy
[d] IC²R srl, Tecnopolis, via Casamassima km 3, Valenzano, Bari 70100, Italy

ARTICLE INFO

Article history:
Received 13 July 2014
Received in revised form
17 September 2014
Accepted 19 September 2014
Available online 28 September 2014

Keywords:
Carbon dioxide reduction
Photocatalysis
Zinc sulfide

ABSTRACT

Industrial utilization of CO_2 is an important research area not only due to the potential contribution to the reduction of emissions into atmosphere, but also for saving carbon resources through the recycle of carbon. The use of solar energy in the conversion of CO_2 appears to be a major challenge and opportunity for the future. A group of nanocrystalline zinc sulfide surface-modified with ruthenium(0) has been designed and characterized. Spectral, structural and electrochemical properties of powders have been determined. Photocatalytic properties of prepared materials were tested towards CO_2 reduction to C_1 compounds. Formic acid and carbon monoxide were found as the major reduction products proving solar to chemical energy conversion. The amount and ratio of products were influenced by the deposited ruthenium(0) co-catalyst and solvent polarity. The mechanism of HCOOH and CO formation, involves a transient $CO_2^{\bullet-}$ radical generation.

1. Introduction

Today most (>85%) of energy used worldwide is produced from fossil fuels. As a consequence, emission of CO_2 into the atmosphere still increases. The perspective of lack of fossil carbon, as well as an increasing level of CO_2 in atmosphere, motivate scientists to search for new methods of CO_2 utilization [1–3]. Among various approaches to CO_2 transformation (catalytic, electrochemical, biochemical, enzymatic) the photocatalytic reduction of carbon dioxide is of a great interest, due to the potential of this method to convert an abundant greenhouse gas to useful products of CO_2 reduction that can be used as fuels or further converted into added value chemicals [4–6].

Semiconductor materials absorb photons producing excitons (electron–hole pairs). Both electrons and holes can participate in interfacial charge transfer processes resulting in primary reduction and oxidation reactions. CO_2 photoreduction at semiconductors has been discussed in several excellent reviews [3,7–10]. Research on this topic was mostly focused on TiO_2-based materials [11–15]. However, CdS, ZnO, ZnS, SiO, Bi_2S_3, Cu_2O, WO_3, $BiVO_4$, Ta_2O_5, Zn_2TiO_4, SiC and graphene oxide were also reported in this context [16–21]. The most commonly tested photocatalyst, *i.e.* commercial TiO_2 P25 (*Evonik*), a typical oxidation photocatalyst shows none or a very low photocatalytic activity towards CO_2 reduction, depending on the experimental conditions [22,23]. Moreover, because of a low efficiency of solar to chemical energy conversion most commonly used semiconducting photocatalysts have to be modified to achieve several goals: (i) photosensitization towards visible light activity (*e.g.* by doping with transition metal cations, adsorption of dyes); (ii) enhanced charge separation (*e.g.* by deposition of metal or semiconductor nanoparticles); (iii) improved catalytic properties (*e.g.* by engineering adsorption properties or deposition of co-catalysts) *etc.* [24–26].

The CO_2 reduction can offer a variety of products. One electron reduction of CO_2 to $CO_2^{\bullet-}$ is a thermodynamically unfavorable reaction. A proton-assisted multielectron reduction of carbon dioxide leads to stable products and therefore such reactions are thermodynamically preferred. The reduction of CO_2 requires a multiple electron transfer and leads to production of a variety of products, depending on the number of transferred electrons, which determine the final oxidation state of the carbon atom. The standard redox potentials of the CO_2 reduction half-reactions vary from −0.61 V for CO_2/HCOOH ($2e^-$ reduction) to −0.24 V for CO_2/CH_4 ($8e^-$ reduction) [27].

* Corresponding author. Tel.: +48 12 663 2222.
E-mail address: macyk@chemia.uj.edu.pl (W. Macyk).

http://dx.doi.org/10.1016/j.apcatb.2014.09.052
0926-3373/

Zinc sulfide is a wide bandgap semiconductor (3.6 eV) that offers a particularly low reduction potential, around −1.8 to −2.0 V *vs.* SHE. The activity of ZnS in photocatalytic water splitting [28,29], carbon dioxide reduction [30–34], coenzyme NADH regeneration [5] and organic synthesis [35–37] has been reported. Due to its reduction properties ZnS seems particularly suitable for CO_2 reduction. A relatively low photostability of ZnS can be overcome by the use of selected electron donors that can efficiently scavenge photogenerated holes, preventing the material from a photocorrosion [38,39]. An efficient hydrogen production, compared to the efficiency of CO_2 reduction, may become another problem related to the use of ZnS-based materials for carbon dioxide reduction processes [30–32].

In aprotic solvents, where no protons can be involved in CO_2 reduction, CO and oxalate are the primary products [40]. Additionally, non-aqueous solvents offer the advantage of a good CO_2 solubility, higher than water.

In recent papers on CO_2 utilization we described systems enabling photocatalytic-enzymatic reduction of CO_2 to methanol [5] and ZnS photocatalysts decorated with ruthenium nanoparticles (Ru@ZnS) active in one electron reduction of CO_2 to $CO_2^{\bullet-}$ [37]. Coupling of $CO_2^{\bullet-}$ to an organic radical, formed upon an organic substrate oxidation with a hole, affords a carboxylic acid molecule. Here we report a multi-electron reduction of carbon dioxide under ultraviolet irradiation in the presence of zinc sulfide materials.

2. Materials and methods

2.1. Preparation of materials

Zinc sulfide (ZnS-A) was prepared according to the method described previously [37]. Under argon atmosphere (Schlenk's system) a solution of Na_2S (0.1 mol) in distilled and deoxygenated water (25 mL) was added dropwise to the aqueous solution of $ZnSO_4{\cdot}H_2O$ (0.1 mol, 25 mL). The mixture was stirred for 24 h. After filtration under argon the powder was washed with water to neutrality and dried at room temperature under vacuum. Another sample of zinc sulfide (ZnS-B) was prepared according to the method described previously [37]. Under nitrogen atmosphere an aqueous solution (20 mL) of NaOH (12.5 mol dm^{-3}) was added dropwise to a solution (20 mL) of $ZnSO_4$ (0.5 mol dm^{-3}). The primarily formed $Zn(OH)_2$ was dissolved as $[Zn(OH)_4]^{2-}$. Then 40 mL of a thiourea solution (0.5 mol dm^{-3}) was added. The obtained mixture was kept at 353 K for 48 h. After separation *via* centrifugation the precipitate was washed with water and ethanol and dried under vacuum. Ruthenium nanoparticles were deposited at the synthesized materials. 1 g of ZnS was suspended in an aqueous solution of $RuCl_3{\cdot}xH_2O$ (10 mL; 10 mmol dm^{-3}) under argon atmosphere. A saturated ethanolic solution of $NaBH_4$ was added dropwise (in excess) under the ultrasonic agitation. Then the powder was filtered off and washed with water under argon. The powder was dried at room temperature under vacuum. Dry materials were stored under nitrogen atmosphere.

2.2. Characterization of materials

UV–vis diffuse reflectance spectra of photocatalysts were recorded using UV-3600 spectrophotometer (*Shimadzu*) equipped with an integrating sphere. Powder samples were ground with $BaSO_4$ (1:50 wt. ratio). Barium sulfate was used as a reference. Prepared materials were analyzed on the X-ray powder diffractometer (MiniFlex 600, *Rigaku*) operated at 40 kV voltage. Energy dispersive X-ray spectra (EDX) were recorded on EDX-720 (*Shimadzu*) spectrometer operated at 5 kV voltage. Scanning electron microscope (Vega 3 LM, *Tescan*), equipped with an LaB_6 cathode and EDS detector (10 mm^2 x-act SDD detector, *Oxford Instruments*), was operated at a voltage of 30 kV.

To describe the redox properties of the materials the spectroelectrochemical determination of its reduction potential was done [41]. The method enables determination of reduction potentials characteristic for the studied material. Both, redox potentials of the conduction band edge and intra-bandgap electronic states, can be determined using this method. Changes in the reflectance upon scanned potential of working electrode (2 cm × 2 cm platinum foil with the casted photocatalyst powder) were recorded with a UV-vis spectrophotometer (Lambda 12, *PerkinElmer*) equipped with a 5 cm dia. integrating sphere, at 700 nm wavelength. A reduction of ZnS results in the increasing absorbance (or decreasing reflectance) at 700 nm. Electrochemical measurements were performed using an electrochemical analyzer (PGSTAT 302 N, *Autolab*) with a three-electrode system (Ag/AgCl, Pt and working electrode; *vide supra*). The electrodes were placed in a quartz cuvette filled with a 0.1 mol dm^{-3} $LiClO_4$ solution in acetonitrile in a way allowing the measurement of the reflectance spectra during the experiment. Oxygen was thoroughly removed from the electrolyte by purging with argon prior to experiments. The range of the applied potential encompassed 0 to −3 V with the scan rate 1 mV s^{-1}.

2.3. Photocatalytic tests

Photocatalytic tests of CO_2 reduction were performed in a quartz cylindrical cuvette (15 mL) equipped with a rubber septum. The photocatalyst (1 g L^{-1}) was suspended in distilled, deoxygenated chloroform or water (5 mL). Isopropanol was used as an electron and proton donor (0.5 mL). Carbon dioxide was bubbled through the suspension for 15 minutes at the ice bath temperature. The suspension was irradiated in the sealed cuvette using 150 W XBO arc lamp as a light source, equipped with the cut-off filter 320 nm. Gas samples were collected at fixed time intervals during irradiation and analyzed by GC (*Thermo Scientific* Focus GC with a TCD detector, helium as the gas carrier and Carboxen-1000 plot column). Using this GC configuration hydrogen, carbon dioxide, carbon monoxide, methane and air as well as vapor of solvent could be analyzed. Liquid samples were filtered through syringe filters (0.22 μm) and analyzed with NMR (*Bruker* 600 MHz).

2.4. Apparent quantum yield measurements

The apparent quantum yield measurements were realized performing the photocatalytic test in a quartz cylindrical cuvette with LED diode (375 nm) as a light source. Ru@ZnS-A (1 g dm^{-3}) was suspended in 5 mL of chloroform. 0.5 mL of isopropanol was added. Noteworthy, isopropanol is used in industry as an H_2-shuttle in hydrogenation reactions. The mixture was irradiated for 1 h. The intensity of light reaching the photoreactor (5 cm^2) was measured with a radiometer Nova II Ophir (*Laser Measurements Group*). The main product (formic acid) was analyzed with ^{1}H NMR (*Bruker* 600 MHz).

3. Results and discussion

ZnS-A and ZnS-B were synthesized according to literature recipes starting from zinc sulfate and sodium sulfide (ZnS-A) or freshly prepared zinc hydroxide and thiourea (ZnS-B) by a hydrothermal route. Metallic ruthenium nanoparticles were deposited at both materials through the impregnation of ZnS powders with ruthenium(III) chloride, followed by its reduction with $NaBH_4$. Since no ruthenium could be detected in the solution after the catalyst centrifugation, almost quantitative deposition

of ruthenium at zinc sulfide samples was assumed. Therefore the resulting materials contained 1% (wt.) of ruthenium.

3.1. Characterization of materials

Diffuse reflectance spectra of the obtained materials have been measured, band gap energies were determined from Tauc plots [42]: 3.47 eV (ZnS-A), 3.57 eV (Ru@ZnS-A), 3.64 eV (ZnS-B), 3.65 eV (Ru@ZnS-B). Modification of the materials with ruthenium does not influence the electronic band structure significantly. Differences in band gap energies between ZnS-A and ZnS-B can be explained by differences in particle sizes (*vide infra*), defects, impurities and disorders in crystal structures which may lead to the formation of additional states within the band gap [43].

Analysis of the chemical composition of photocatalysts was carried out by X-ray diffraction spectroscopy (XRD) and energy dispersive X-ray spectroscopy (EDX). XRD analysis, shown in Fig. 1, proves the zinc blende structure (sphalerite) of both ZnS-A and ZnS-B materials (JCPDS No. 05–0566) [44]. Particle sizes calculated from XRD measurements (using the Scherrer's equation) are equal to 3.3 and 20.6 nm for ZnS-A and ZnS-B, respectively, as calculated basing on the most intense peak $2\Theta = 28^{\circ}$. Dynamic light scattering measurements allow to classify ZnS-B as the material composed of bigger aggregates (*ca.* 350 nm) when compared to particles of ZnS-A (*ca.* 300 nm), in accordance with previously reported data [37]. Ruthenium deposition results in bigger aggregates formation: 350 and 460 nm for Ru@ZnS-A and Ru@ZnS-B, respectively. Deposition of ruthenium particles increases the average size of nanoparticles by about 0.6 nm. Energy dispersive X-ray analysis confirmed the presence of ruthenium particles on ZnS surface based on 2.56 and 19.27 keV signals (data presented elsewhere [37]).

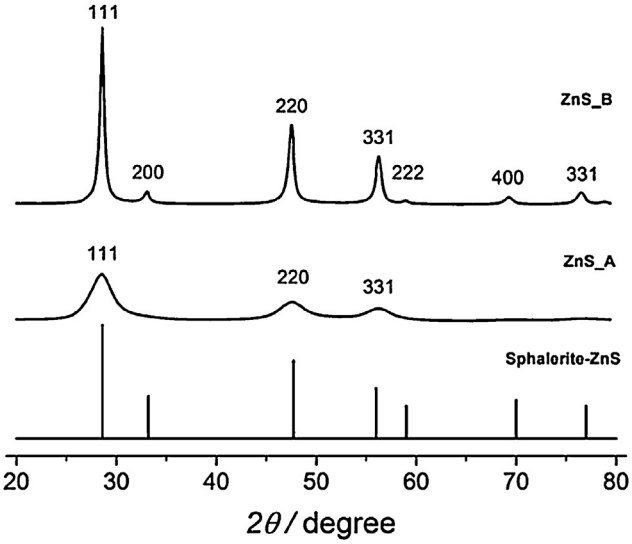

Fig. 1. XRD patterns of ZnS-A and ZnS-B compared with data for sphalerite (JCPDS No. 05-0566).

The specific surface areas of the synthesized photocatalysts are relatively high in the case of ZnS-A materials (105 and 78 $m^2\ g^{-1}$ for ZnS-A and Ru@ZnS-A, respectively) and *ca.* twice lower for ZnS-B (56 and 55 $m^2\ g^{-1}$ for ZnS-B and Ru@ZnS-B, respectively). The specific surface areas of ZnS samples loaded with ruthenium is reduced

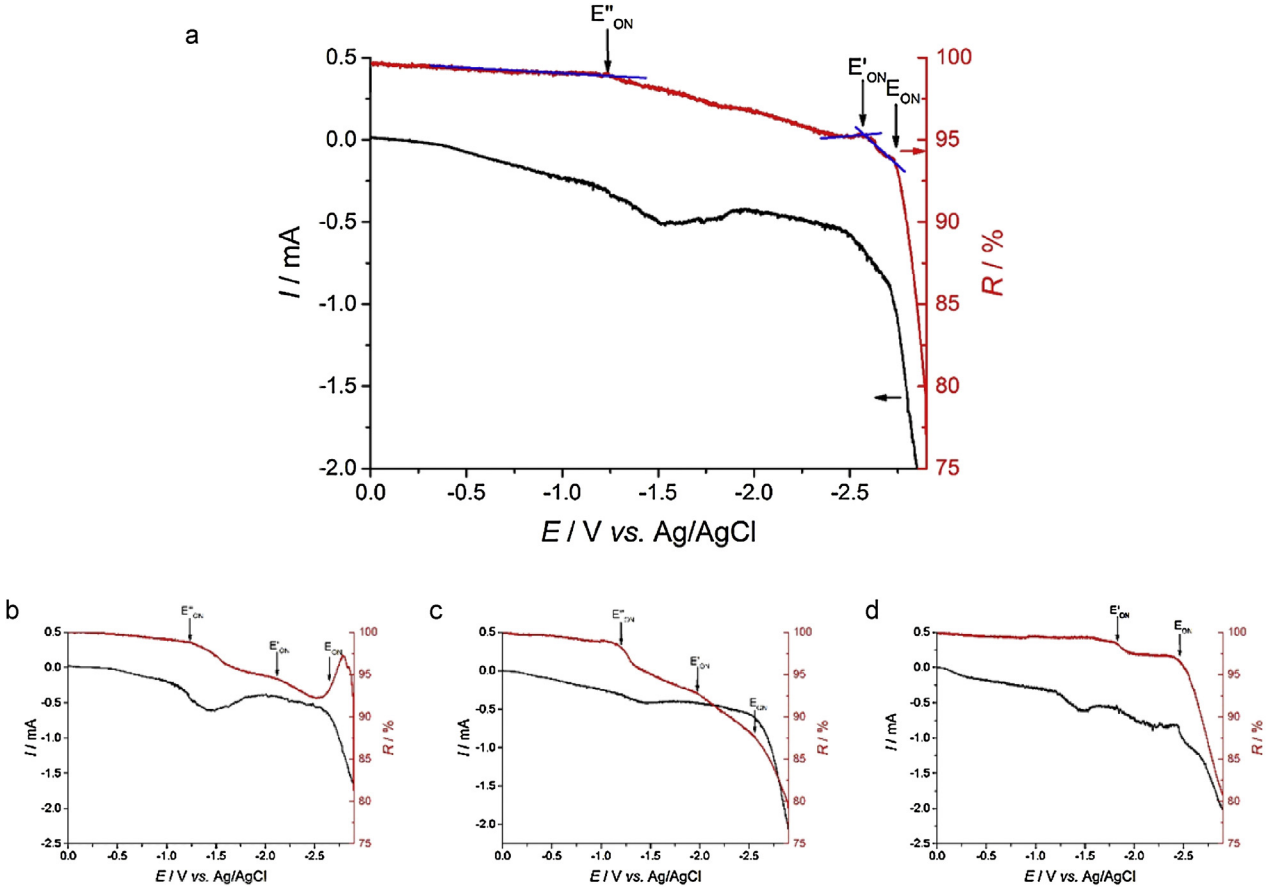

Fig. 2. Current (black lines) and reflectance (red lines) changes upon swept potential for working electrodes made of ZnS-B (a), ZnS-A (b), Ru@ZnS-A (c), and Ru@ZnS-B (d). Materials deposited on platinum foil, 0.1 mol dm^{-3} $LiClO_4$ solution in anhydrous acetonitrile.

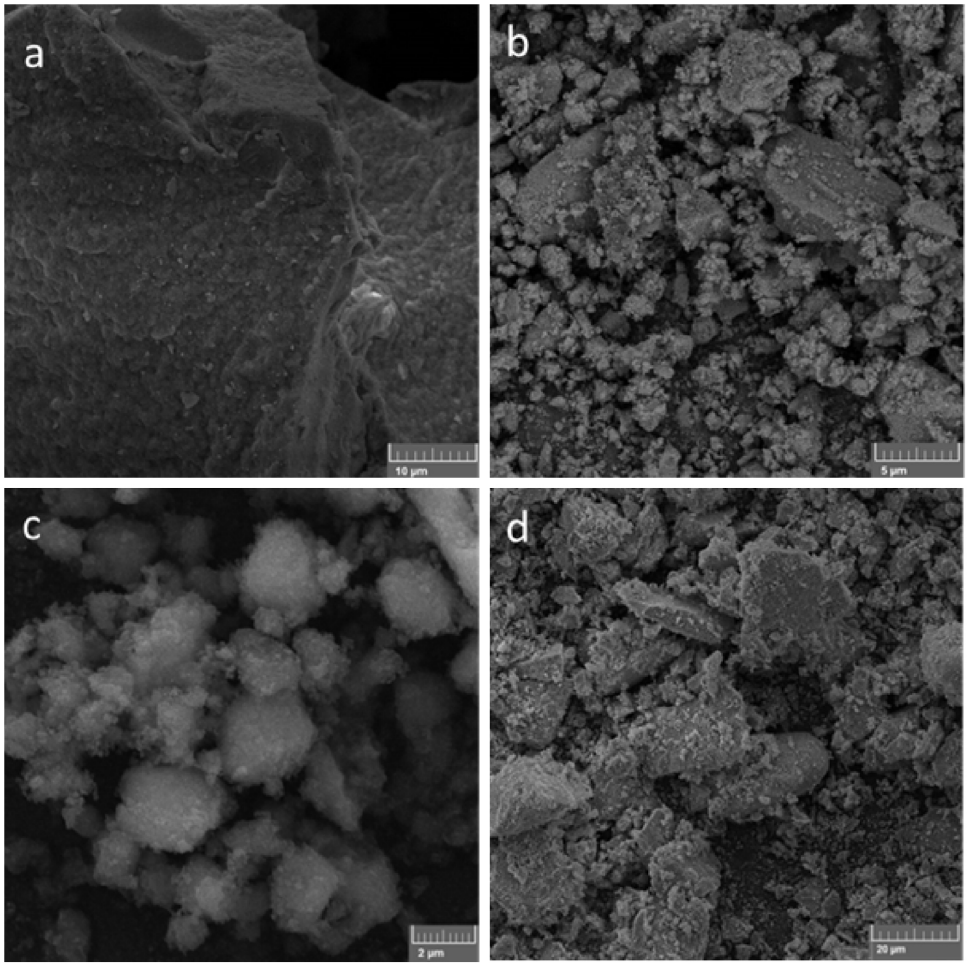

Fig. 3. SEM images of ZnS-A (a), Ru@ZnS-A (b), ZnS-B (c), Ru@ZnS-B (d).

comparing with starting materials. This decrease can be attributed to a stronger aggregation of nanoparticles observed upon deposition of ruthenium (*vide supra*) and to blocking of some pores, particularly in the case of ZnS-A.

The results of spectroelectrochemical measurements are shown in Fig. 2 and Table 1. Changes of current and reflectance upon swept potential allow to determine potentials of conduction band edge and electronic states lying beneath [41]. The potential at which electrons start to be trapped (E_{ON}) may be determined from $R(E)$ plot. E_{ON} describes the material ability to accept electrons into the conduction band. The potentials of conduction band edges vary for the studied materials between −2.3 and −2.6 V *vs.* SHE, reaching higher values in the case of samples decorated with ruthenium (E_{ON} values in Table 1 and Fig. 2). ZnS-A materials offer slightly better reducing properties when compared to ZnS-B. Beside the main reduction potential all materials can accept electrons in intra-bandgap electronic states, as depicted in Fig. 2. The intra-bandgap states are localized within a broad range of −1.0 to −2.4 V *vs.* SHE. The deeper electronic states are less influenced by the presence of ruthenium than those localized closer to the conduction band (compare ZnS-A and Ru@ZnS-A).

Table 1
Electronic states values for the studied materials with respect to an SHE electrode.

Material	E_{ON}, *V vs.* SHE (±0.1 V)	Other electronic states, *V vs.* SHE (±0.1 V)
ZnS-A	−2.6	−1.9; −1.0
Ru@ZnS-A	−2.5	−1.8; −1.0
ZnS-B	−2.5	−2.4; −1.0
Ru@ZnS-B	−2.3	−1.6

Fig. 3 shows the SEM images of the photocatalysts. The materials are composed of irregular aggregates (0.2–2.0 μm) of smaller nanoparticles.

3.2. Photocatalytic activity

The activity of materials has been tested in photocatalytic reduction of carbon dioxide. Irradiation of the suspensions of prepared materials saturated with carbon dioxide resulted in the reduction of CO_2 to formic acid, carbon monoxide and methane, as demonstrated by GC and ^{1}H NMR analyses. Fig. 4 summarizes the results obtained after 5 h of irradiation in the presence of neat ZnS-A and ZnS-B, as well as the materials modified with ruthenium, showing also the amounts of formed hydrogen. Formic acid (in liquid) and carbon monoxide (in gas phase) were the main products of CO_2 reduction in the case of both, modified and unmodified photocatalysts. Small quantities of methane have been also detected in the gas phase above the reaction mixture. Noteworthy, the selectivity of the formate production at ZnS-A is very high. Additionally, formation of acetone, as the product of electron donor (2-propanol) oxidation, and hydrogen, was observed. Neither oxalic acid nor oxalate has been found basing on ^{13}C NMR analyses. The reaction did not proceed in systems lacking any of the following components: the photocatalyst, light or carbon dioxide (instead of saturation with CO_2, the mixture was saturated with argon). The lack of any reduction products in the case of the reference tests

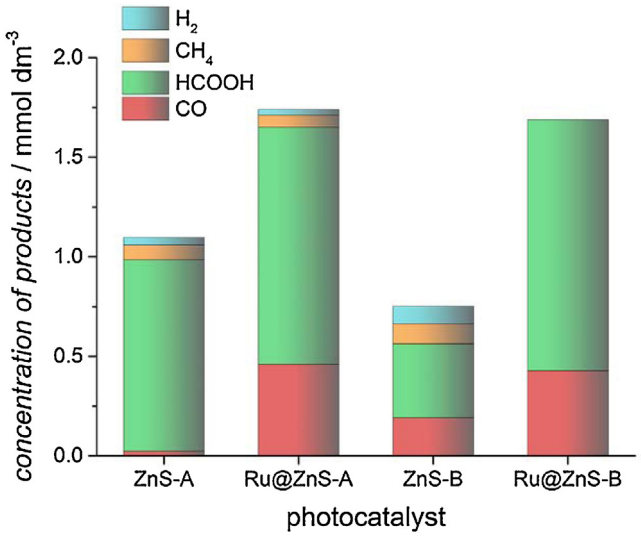

Fig. 4. Products found in the reaction mixture after 5 h irradiation of the photocatalyst suspension in the presence of isopropanol (UV light, $[i\text{-PrOH}]_0 = 1.2\ mol\ dm^{-3}$, $c_{photocat} = 1\ g\ dm^{-3}$).

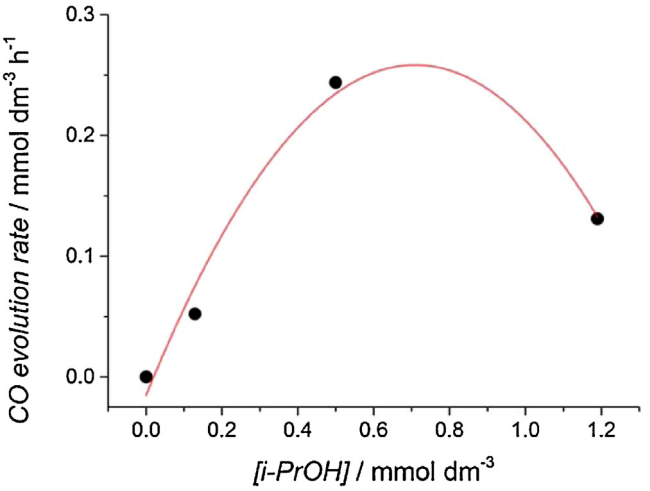

Fig. 6. The rate of CO evolution as a function of isopropanol concentration measured in the presence of ZnS-B. Irradiation time – 1 h.

performed in the absence of carbon dioxide, but in the presence of all other components, including photocatalysts and isopropanol, points at CO_2 as the source of products. Therefore the possibility of isopropanol oxidation to C_1 compounds can be ruled out. The amount of produced hydrogen is low in comparison with other products for all tested materials. Moreover, materials modified with ruthenium showed even lower (or negligible) activity towards H_2 formation when compared to the neat photocatalysts. Commercially available titanium dioxide (P25, *Evonik*) shows a negligible activity under the same reaction conditions. The amounts of products were below the limit of quantification.

The calculated apparent quantum yields of CO_2 conversion to formic acid at 375 nm in the presence of the most efficient photocatalyst (Ru@ZnS-A) is equal to 0.50% (±0.05%). The apparent quantum yield is often used to characterize heterogeneous photosystems, where determination of the number of absorbed photons is difficult or impossible. Calculations of apparent quantum yields are based assuming absorption of all incident light [45]. Since this assumption overestimates the number of absorbed photons, the real quantum yield is higher than the measured apparent quantum yield.

Materials modified with ruthenium (Ru@ZnS-A and Ru@ZnS-B) appeared more efficient in the process of CO_2 reduction than neat materials (ZnS-A and ZnS-B) under identical reaction conditions. In their presence the higher production of both main products, carbon monoxide and formic acid, was observed. A positive influence of ruthenium modifier may originate from: (i) a catalytic effect (lowering the CO_2 activation energy); (ii) collection of electrons at Ru particles resulting in a better charge separation (increased lifetimes of photogenerated charges) and improved multielectron reduction process; (iii) a significantly better adsorption of CO_2 at the surface of modified materials, as confirmed experimentally elsewhere [37]. Materials with deposited ruthenium appear also more selective towards formic acid formation. Production of HCOOH is particularly efficient within the first hour of irradiation (Fig. 5). This observation may be explained by poisoning of the catalyst, oxidation of ruthenium or detaching the ruthenium nanoparticles from the surface of ZnS. In the case of reaction at Ru@ZnS-B (right graph in Fig. 5) the formation of carbon monoxide during the first hour of irradiation is higher than in the case of reaction photocatalyzed by neat

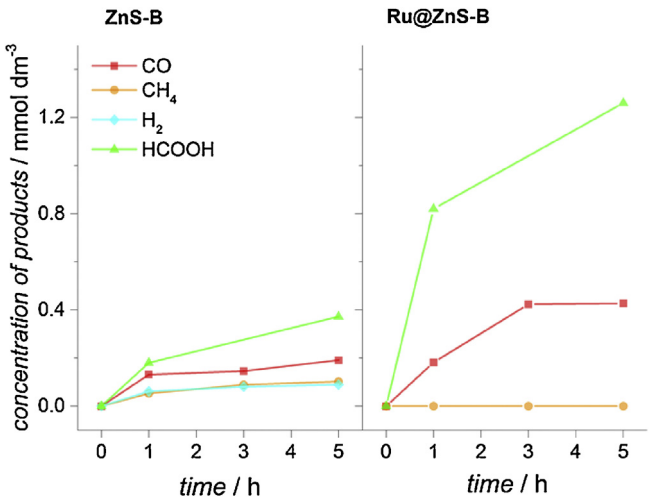

Fig. 5. Evolution of hydrogen and CO_2 photoreduction products in the presence of ZnS-B and Ru@ZnS-B.

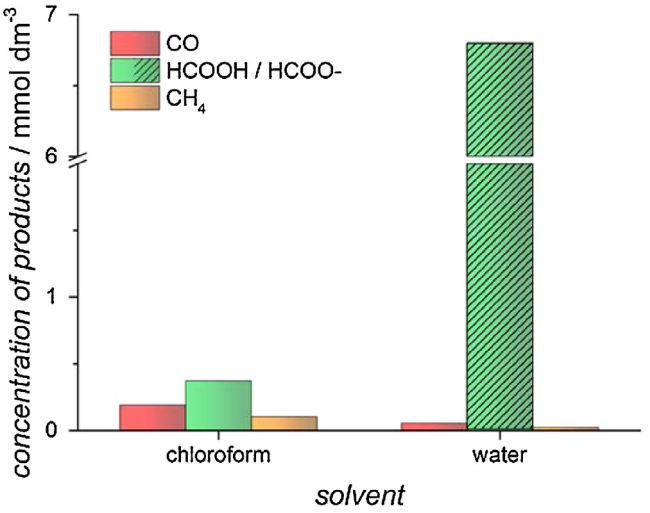

Fig. 7. Photoreduction of CO_2 after 5 h of irradiation in $CHCl_3$ and H_2O in the presence of ZnS-B.

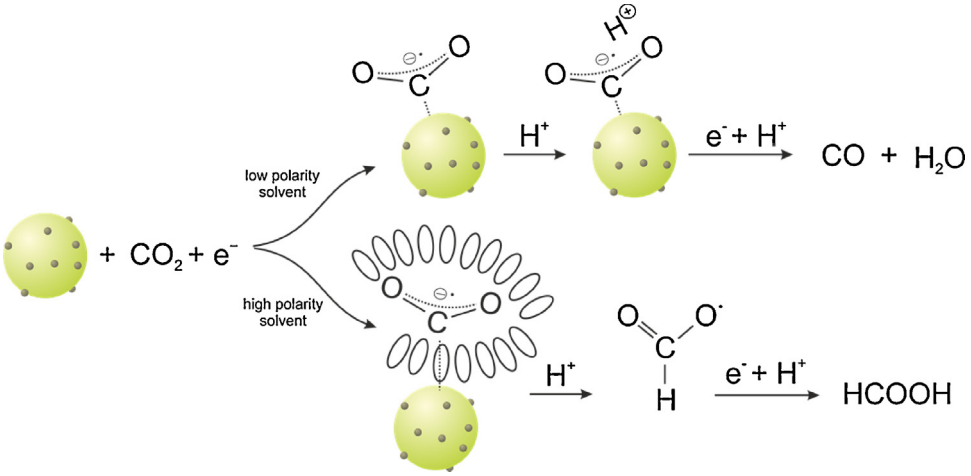

Fig. 8. Possible mechanisms of CO_2 reduction in low and high polarity solvents. Adopted from [46].

ZnS-B. Methane was not formed when Ru@ZnS-B was used. Similar observations are also valid for materials based on ZnS-A.

Fig. 6 shows the influence of electron donor concentration on reaction efficiency. Isopropanol plays the role of a sacrificial electron donor, therefore an increase of the isopropanol concentration enhances the reaction rate up to [iPrOH][*i*-PrOH] = 0.7 mol dm^{-3}. At higher concentrations the reaction slows down. The reaction rate has been defined here as the change of carbon monoxide concentration during 1 hour irradiation of the reaction mixture.

The effect of various solvents on photocatalytic reduction of carbon dioxide was tested using neat ZnS-B photocatalyst (Fig. 7). In water (high polarity solvent) only traces of CO were formed, while formic acid is the dominating product. In the case of chloroform (low polarity solvent) the overall efficiency of CO_2 reduction is much lower, however the CO formation yield is higher than in water. It is worth to emphasize that water reveals to be a better H-transfer agent than isopropanol (*cf.* Fig. 4) with a HCOOH yield some three-four times higher with the same photocatalyst. Such behavior is not usual.

As recently proven by EPR spin-trapping experiments, $CO_2^{\bullet-}$ is photogenerated in the presence of both ZnS and Ru@ZnS materials [37]. Differences in relative efficiencies of $HCOO^-$ and CO formation in various solvents can be explained by generation of $CO_2^{\bullet-}$ and its successive reduction with the second electron. In low polarity solvents the formed carbon dioxide anion radical can be strongly adsorbed at the surface of photocatalyst due to a poor solvation [46]. Upon double protonation and the second reduction step CO and H_2O are formed. In polar solvents another mechanism prevails – $CO_2^{\bullet-}$ is stabilized by solvent molecules which, upon protonation and further reduction-protonation, is transformed to formic acid (Fig. 8). Interestingly, both reduction processes are formally "$2e^- + 2H^+$" transfer to CO_2, however, the polarity of the reaction medium drives the reaction towards one of the reactions.

4. Conclusions

ZnS-A and ZnS-B were prepared according to the various procedures. Both materials have been functionalized by deposition of ruthenium nanoparticles. Obtained photocatalysts show differences in the electronic band structure, morphology, as well as in the photocatalytic activity. They are characterized by a low redox potential of the conduction band edge, as determined by spectroelectrochemical measurements. The prepared ZnS-based photocatalysts, in particular Ru@ZnS, photocatalyze CO_2 reduction to formic acid (in liquid phase), carbon monoxide (gas phase) and traces of methane (gas phase). The differences in particle sizes may be responsible for different activity of ZnS-A and ZnS-B. Nanocrystalline ZnS-A (3.3 nm) shows a slightly higher activity toward CO_2 photoreduction than ZnS-B (20.6 nm). The particle size influences many other fundamental properties of photocatalysts, namely the specific surface area, potentials of bands edges, the spectral range of absorbed light or even lifetime of photogenerated charges. Ruthenium particles deposited at the surface of zinc sulfide may act as a catalyst (lowering the activation energy, improving adsorption of CO_2), or act as an electron sink (increasing the life time of photogenerated charges).

Ultraviolet irradiation induces the direct electron transfer from the valence to conduction band of ZnS. The separated electrons and holes participate in redox reactions at the surface of photocatalyst. The photoinduced reduction encompasses a cleavage of C–O bonds or formation of C–H, leading to CO or HCOO−, respectively (Eqs. (1) and (2)):

$$CO_2 + \xrightarrow{e^-_{CB}} CO^{\bullet-}_{2\,(ads)} \xrightarrow{e^-_{CB}+2H^+} CO + H_2O$$

(prevailing in non-polar solvents) (1)

$$CO_2 + \xrightarrow{e^-_{CB}} CO^{\bullet-}_{2\,(sol)} \xrightarrow{H^+} O\dot{C}OH \xrightarrow{e^-_{CB}+H^+} HCOOH$$

(prevailing in polar solvents) (2)

An extremely low redox potential of the bottom of conduction band (−2.5 V *vs.* SHE) enables one-electron reduction of carbon dioxide to $CO_2^{\bullet-}$. Formation of carbon dioxide anion radical has been confirmed by EPR spectroscopy (spin trapping experiments), as described elsewhere [37]. Transformations of CO_2 to HCOOH and CO are two-electron processes. A further reduction to formaldehyde or methanol is less favorable. Isopropanol acts as an electron donor yielding acetone (confirmed by ^{13}C NMR, data not shown):

$$(CH_3)_2CHOH + 2h^+ \rightarrow (CH_3)_2CO + 2H^+ \quad (3)$$

In conclusion, ZnS photocatalysts functionalized with ruthenium nanoparticles were found to be active in photocatalytic CO_2 reduction to C_1 products of two-electron reduction. Small amounts of methane prove a capability of the materials to photocatalyze other multielectron reduction processes, however the presented data prove a possibility of a highly selective production of formate in aqueous media. A low efficiency of the hydrogen production and therefore a high selectivity of carbon dioxide reduction, in particular in water, is an important advantage of the described

systems. The redox properties of ZnS, *i.e.* a particularly low potential of the conduction band edge, make this material very different from titanium dioxide. A relatively low photostability of ZnS may be overcome by the use of electron donors that can efficiently pick up photogenerated holes preventing the material photocorrosion.

Acknowledgements

The support from the Foundation for Polish Science within the VENTURES/2011-8/1 Project and the Project TEAM/2012-9/4, both co-financed by the EU European Regional Development Fund, is highly acknowledged. IC^{2}R is thankfully acknowledged for a financial support.

Appendix A. Supplementary data

Supplementary data associated with this article can be found, in the online version, at http://dx.doi.org/10.1016/j.apcatb.2014.09.052.

References

[1] A. Dibenedetto, M. Aresta, in: P. Imhof, J.C. van der Waal (Eds.), Catalytic Process Development for Renewable, Wiley-VCH Verlag GmbH & Co. KGaA, Weinheim, Germany, 2013, http://dx.doi.org/10.1002/9783527656639.ch13.
[2] M. Aresta, A. Dibenedetto, A. Angelini, J. CO_2 Util. 3–4 (2013) 65–73.
[3] M. Aresta, A. Dibenedetto, A. Angelini, Chem. Rev. 114 (2014) 1709–1742.
[4] C. Shi, H.A. Hansen, A.C. Lausche, J.K. Nørskov, PCCP 16 (2014) 4720–4727.
[5] A. Dibenedetto, P. Stufano, W. Macyk, T. Baran, C. Fragale, M. Costa, M. Aresta, ChemSusChem 5 (2012) 373–378.
[6] F.J. Fernández-Alvarez, A.M. Aitani, L.A. Oro, Catal. Sci. Technol. 4 (2014) 611–624.
[7] S.N. Habisreutinger, L. Schmidt-Mende, J.K. Stolarczyk, Angew. Chem. Int. Ed. 52 (2013) 7372–7408.
[8] S.C. Roy, O.K. Varghese, M. Paulose, C.A. Grimes, ACS Nano 4 (2010) 1259–1278.
[9] T. Yui, Y. Tamaki, K. Sekizawa, O. Ishitani, Top. Curr. Chem. 303 (2011) 151–184.
[10] S. Navalón, A. Dhakshinamoorthy, M. Álvaro, H. Garcia, ChemSusChem 6 (2013) 562–577.
[11] M. Manzanares, C. Fàbrega, J. Oriol Ossó, L.F. Vega, T. Andreu, J.R. Morante, Appl. Catal. B: Environ. 150–151 (2014) 57–62.
[12] C.-W. Lee, R. Antoniou Kourounioti, J.C.S. Wu, E. Murchie, M. Maroto-Valer, O.E. Jensen, C.-W. Huang, A. Ruban, J. CO_2 Util. 5 (2014) 33–40.
[13] J. Mao, L. Ye, K. Li, X. Zhang, J. Liu, T. Peng, L. Zan, Appl. Catal. B: Environ. 144 (2014) 855–862.
[14] S. Rani, N. Bao, S.C. Roy, Appl. Surf. Sci. 289 (2014) 203–208.
[15] K. Kočí, L. Obalová, L. Matějová, D. Plachá, Z. Lacný, J. Jirkovský, O. Šolcová, Appl. Catal. B: Environ. 89 (2009) 494–502.
[16] J. Chen, S. Qin, G. Song, T. Xiang, F. Xin, X. Yin, Dalton Trans. 42 (2013) 15133–15138.
[17] J. Yu, J. Jin, B. Cheng, M. Jaroniec, J. Mater. Chem. A 2 (2014) 3407–3416.
[18] A.D. Handoko, J. Tang, Int. J. Hydrogen Energy 38 (2013) 13017–13022.
[19] P.-Q. Wang, Y. Bai, P.-Y. Luo, J.-Y. Liu, Catal. Commun. 38 (2013) 82–85.
[20] T.M. Suzuki, T. Nakamura, S. Saeki, Y. Matsuoka, H. Tanaka, K. Yano, T. Kajino, T. Morikawa, J. Mater. Chem. 22 (2012) 24584–24590.
[21] M.A. Gondal, M.A. Ali, X.F. Chang, K. Shen, Q.Y. Xu, Z.H. Yamani, J. Environ. Sci. Health Part A: Tox. Hazard. Subst. Environ. Eng. 47 (2012) 1571–1576.
[22] J. Fu, S. Cao, J. Yu, J. Low, Y. Lei, Dalton Trans. 43 (2014) 9158–9165.
[23] B. Michalkiewicz, J. Majewska, G. Kądziołka, K. Bubacz, S. Mozia, A.W. Morawski, J. CO_2 Util. 5 (2014) 47–52.
[24] M. Buchalska, J. Kuncewicz, E. Świętek, P. Łabuz, T. Baran, G. Stochel, W. Macyk, Coord. Chem. Rev. 257 (2013) 767–775.
[25] J. Yang, D. Wang, H. Han, C. Li, Acc. Chem. Res. 46 (2013) 1900–1909.
[26] S. Banerjee, S.C. Pillai, P. Falaras, K.E. O'Shea, J.A. Byrne, D.D. Dionysiou, J. Phys. Chem. Lett. 5 (2014) 2543–2554.
[27] E. Fujita, Coord. Chem. Rev. 185–186 (1999) 373–384.
[28] E. Baniasadi, I. Dincer, G.F. Naterer, Appl. Catal. Gen. 455 (2013) 25–31.
[29] G.-J. Lee, S. Anandan, S.J. Masten, J.J. Wu, Ind. Eng. Chem. Res. 53 (2014) 8766–8772.
[30] K. Kočí, L. Matějová, O. Kozák, L. Čapek, V. Valeš, M. Reli, P. Praus, K. Šafářová, A. Kotarba, L. Obalová, Appl. Catal. B: Environ. 158–159 (2014) 410–417.
[31] K. Kočí, M. Reli, O. Kozák, Z. Lacný, D. Plachá, P. Praus, L. Obalová, Catal. Today 176 (2011) 212–214.
[32] O. Kozák, P. Praus, K. Kočí, M. Klementová, J. Colloid Interface Sci. 352 (2010) 244–251.
[33] H. Fujiwara, H. Hosokawa, K. Murakoshi, Y. Wada, S. Yanagida, Langmuir 14 (1998) 5154–5159.
[34] R. Zhou, M.I. Guzman, J. Phys. Chem. C 118 (2014) 11649–11656.
[35] M. Gartner, J. Ballmann, C. Damm, F.W. Heinemann, H. Kisch, Photochem. Photobiol. Sci. 6 (2007) 159–164.
[36] G. Hörner, P. Johne, R. Künneth, G. Twardzik, H. Roth, T. Clark, H. Kisch, Chem. Eur. J. 5 (1999) 208–217.
[37] T. Baran, A. Dibenedetto, M. Aresta, K. Kruczała, W. Macyk, ChemPlusChem 79 (2014) 708–715.
[38] H. Yoneyama, Catal. Today 39 (1997) 169–175.
[39] P. Johne, H. Kisch, J. Photochem. Photobiol. A: Chem. 111 (1997) 223–228.
[40] E. Barton Cole, A.B. Bocarsly, in: M. Aresta (Ed.), Carbon Dioxide Chem. Feedstock, Wiley-VCH Verlag GmbH & Co. KGaA, 2010, pp. 291–316.
[41] E. Świętek, K. Pilarczyk, J. Derdzińska, K. Szaciłowski, W. Macyk, PCCP 15 (2013) 14256–14261.
[42] J. Tauc, Mater. Res. Bull. 5 (1970) 721–729.
[43] D.H. Hwang, J.H. Ahn, K.N. Hui, K.S. Hui, Y.G. Son, Nanoscale Res. Lett. 7 (2012) 26.
[44] Y. Chen, Q. Wu, Y. Ding, J. Braz. Chem. Soc. 18 (2007) 924–927.
[45] M. Kaneko, I. Okura, Photocatalysis: Science and Technology, Springer, 2002.
[46] B.-J. Liu, T. Torimoto, H. Matsumoto, H. Yoneyama, J. Photochem. Photobiol. A:Chem. 108 (1997) 187–192.